Acoustic Wavefields Simulation by the Ray Method with Approximation of a Broadband Signal Propagation

Dmitry Neklyudov(✉) and Maxim Protasov

Institute of Petroleum Geology and Geophysics SB RAS, prosp. acad. Koptuga 3, Novosibirsk 630090, Russia
neklyudovda@ipgg.sbras.ru

Abstract. The paper presents a method for calculating frequency-dependent rays, which allows effective approximation of a broadband signal propagation. We provide comparative analysis of this method with the standard ray method and the finite-difference method. The developed algorithm is promising for modelling and inverse problems. We performed the numerical examples for the realistic Sigsbee model.

Keywords: Ray method · Broadband signal · Green function

1 Introduction

Asymptotic methods play an important role in solving direct and inverse problems in seismic. The ray method occupies a special place among them [1–3]. Based on it, key procedures for processing seismic data and constructing seismic images, such as Kirchoff depth migration, are implemented [4–6]. The ray method is used to calculate the travel times of seismic waves. However, it is also used to calculate wave fields in models with a moderate complexity. An important limitation of the ray method is the fact that it is based on a high-frequency approximation of signal propagation processes. It does not consider that the real seismic signals are broadband and have a limited spectrum [7, 8]. A high-frequency approximation often leads to "unphysical" behavior of the rays and the corresponding travel times calculated along the ray trajectories in models with sharp interfaces between regions with different values of physical parameters. The limited spectrum signals propagate within some volume surrounding the ray (the so-called Fresnel zone or in 3D "Fresnel volume"). Dominant frequency of the signal determines the width of this volume. The signal "feels" variations in the parameters of the medium within this volume and changes the direction of its propagation accordingly, [9, 10].

Several approaches can take the band limited waves nature into account with varying degrees of efficiency and weaken the influence of the high-frequency approximation used in the ray method [11–18]. The papers [19–21] consider the so-called "exact" frequency-dependent rays. They show such rays provide an efficient calculation of the

© The Author(s), under exclusive license to Springer Nature Switzerland AG 2022
O. Gervasi et al. (Eds.): ICCSA 2022, LNCS 13376, pp. 84–96, 2022.
https://doi.org/10.1007/978-3-031-10450-3_7

travel times under salt bodies. However, "exact" frequency-dependent rays are computationally expensive, since the procedure requires knowledge of acoustic wavefield for a given frequency. Another approach proposed in [12] and considered in [22] is a simplified but highly effective method for approximating the propagation of broadband seismic signals in complex environments. The author (A. Lomax) calls it "the wavelength-smoothing technique". The method is based on the use of the Huygens's principle and the frequency-dependent velocity function. The key point of Lomax method is the fact that velocity used for ray tracing is determined by smoothing actual velocity along the normal to the ray at the current point over an aperture proportional to the wavelength (i.e. along some pre-defined portion of the wave front). Below we will call the rays constructed by this method as "Lomax rays". In the limiting case when the wavelength becomes infinite small, Lomax rays reduces to the standard rays described by classical ray theory. In this paper, we prove that Lomax rays might be quite promising in some seismic exploration applications. Particularly, we demonstrate the use of Lomax rays to calculate travel times and acoustic wave fields in complex environments and compare these results with results provided by much more computationally expensive finite-difference method for two-way acoustic wave equation.

2 Lomax Ray Calculation

In this section, we briefly present the algorithm for Lomax rays calculation and emphasize what exactly is their difference from standard rays. For a clearer presentation, we will focus on the two-dimensional case. All the above arguments work for the three-dimensional case. The key point in the Lomax method is velocity smoothing along the current position of the front (more precisely, in the normal direction to the ray). For the given frequency υ (we consider it as a certain parameter for now) the average velocity has the expression,

$$v_{sm}\left(\vec{x}_p, v\right) = \frac{\sum_{j=-N}^{N} w_j \cdot v(\vec{x}_j)}{\sum_{j=-N}^{N} w_j} \tag{1}$$

where w_j are the values of the smoothing function (we will mention this later), $v(\vec{x}_j)$ is the values of the velocities taken at certain points $\vec{x}_j$ along the front. These points are located symmetrically regarding the central point $\vec{x}_p = (x_p, z_p)$. The maximum distance from the central point (averaging aperture) is determined by the parameter θ, which is specified in wavelengths, $\theta \sim \lambda$, where $\lambda = \frac{v(\vec{x}_p)}{\upsilon}$, (for example $\theta = 1.5$). As a smoothing function, we use the Gaussian function (other options are possible): $w(x) = \exp\left\{-4\ln 2\left(\frac{x}{2}\right)^2\right\}$.

Let a Lomax is constructed at some point $\vec{x}_p = \left(x_p, z_p\right)$. At this point a unit tangent vector $\vec{s} = (s_x, s_z)$ is given. The unit normal to the ray is $\vec{n} = (s_z, -s_x)$. In the normal direction $\vec{n}$, at a distance l from a central point on the ray, we define edge points $\vec{x}_1$ and $\vec{x}_2$ symmetrically (Fig. 2). At each of the three points, we calculate smoothed velocities using the expression (1): $\overline{v}_p = v_{sm}(\vec{x}_p, v)$, $\overline{v}_1 = v_{sm}(\vec{x}_1, v)$, $\overline{v}_2 = v_{sm}(\vec{x}_2, v)$. We use the same direction of smoothing along the normal $\vec{n}$ for the edge points $\vec{x}_1, \vec{x}_2$. Let us define

the time step along the ray as dt. During this time, the central point $\vec{x}_p$ moves to the point $\vec{x}_p + d\vec{x}_p$, $d\vec{x}_p = (dx_p, dz_p)$ along the vector $\vec{s}$:

$$dx_p = \overline{v}_p dt \cdot s_x, dz_p = \overline{v}_p dt \cdot s_z \tag{2}$$

The edge points move respectively at the distance $\overline{v}_1 dt$, $\overline{v}_2 dt$ (Fig. 2). Assuming that the front remains locally flat, from simple geometric considerations, one can get an expression for the correction to the tangent vector to the ray $d\vec{s}$ and find the tangent vector at the next point on the ray (Fig. 2):

$$ds_x = -\frac{d\overline{v}_p}{x_1 - x_2} dt \cdot s_z, ds_x = -\frac{d\overline{v}_p}{z_1 - z_2} dt \cdot s_x, d\overline{v}_p = \overline{v}_1 - \overline{v}_2 \tag{3}$$

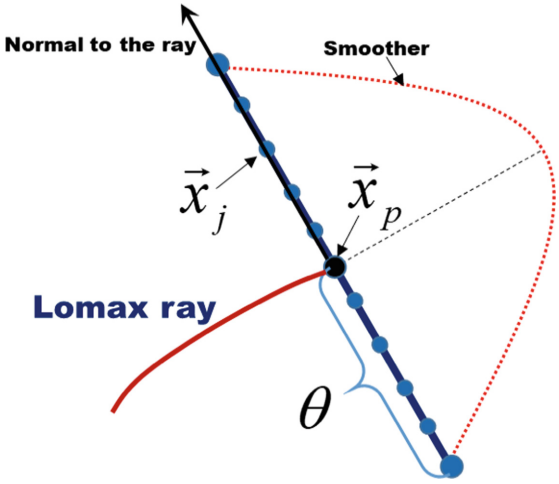


Fig. 1. Smoothing velocity along a ray normal vector.

Thus, there is a step-by-step movement along the ray. Note that the "Lomax" ray tracing is performed in a certain volume of the medium. Simultaneous movement of three points determines a next position of the front. The parameter l (the width of the flat front) turns out to be a very important parameter. We propose to determine it adaptively at each time step along the ray, dt, depending on the wavelength: $l = q \cdot \lambda$, where $q \sim 0.25 - 0.5$.

In the limit case, $l \to 0, dt \to 0$ one obtain a system of ordinary differential equation of Lomax ray:

$$\frac{d\vec{s}}{dt} = -(\nabla \bar{v}_p \cdot \vec{n})\vec{n}, \quad \frac{\vec{dx}}{dt} = \bar{v}_p \vec{s} \tag{4}$$

Equations (4) become equivalent to the equations of standard ray tracing when the averaged velocity $\bar{v}_p$ is replaced by the local velocity $v(\vec{x})$.

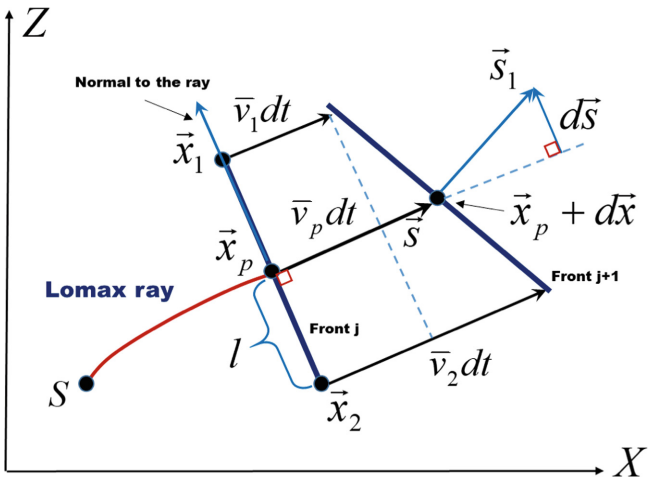


Fig. 2. Lomax ray calculation (scheme).

When constructing rays, we determine the traveltimes at the points of the medium through which each ray passes. Below, we need to determine the traveltimes on some regular grid. With Lomax rays, considering the specifics of their construction, it is possible to propose a natural algorithm for interpolating traveltimes given at irregularly spaced points on a ray to a regular grid. When constructing a Lomax ray, at each point of the ray, a certain volume of the medium is considered, which is determined by the wavelength at the current point. Let us calculate the ray. Moving along the ray, i.e. increasing traveltime by a constant increment dt, consider the position at time T_j. When constructing the ray up to the moment of time $T_{j+1} = T_j + dt$, the flat wavefront has passed through the area of the medium, concentrated inside the trapezoid. The bases of the trapezoid are two segments: the position of the front at the moment T_j and the position of the front at the moment T_{j+1} (Fig. 3). The points of a regular grid may be located inside this trapezoid. When such points are found, then the traveltimes are interpolated in these points according to the principle shown schematically in Fig. 3.

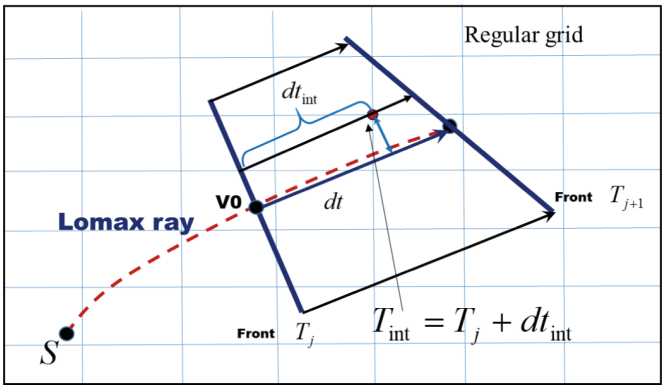


Fig. 3. Interpolation of traveltimes to a regular grid in Lomax ray tracing.

3 Green's Function Calculation

In this section, we present the formulas needed to calculate the Green's functions in the frequency domain by the ray method. Such a problem may arise, for example, when asymptotic methods are used for wavefields simulation in full-waveform inversion [23]. For such a problem, it is necessary to calculate a Green's function at a frequency ω on a regular grid with a fixed source position (x_S, z_S), i.e.$G(x, z, x_S, z_S; \omega)$. In the two-dimensional case, the expression for the Green's function calculated at point R with the source in the point S is defined as [3, 24]:

$$G(R; S) = S(\omega)A(S, R)\exp\{i\omega\tau(S, R)\}, \tag{5}$$

where $\tau(S, R)$ is traveltime along a ray between the points S and R, the multiplier $S(\omega) = \sqrt{\frac{1}{-i\omega}}$, $A(S, R)$ is an amplitude factor provided by the ray method:

$$A(S, R) = \sqrt{\frac{v(R)}{8\pi v(S) \cdot J(S, R)}}, \tag{6}$$

$v(S)$ is a value of velocity in corresponding point of velocity model, $J(S, R)$ is geometrical spreading along a ray:

$$J \sim \frac{\delta L}{\delta\theta_S}, \tag{7}$$

where δL is a width of a ray tube in point R, $\delta\theta_S$ is an opening angle increment in the initial point of the ray tube (see Fig. 4).

Having several rays calculated for a source position within the whole computational domain, it is possible to evaluate approximately the Green's function using the formulas (5–7), [3]. Since we use the approximate expression for geometrical spreading (7), ray coverage (or ray density) within the target area should be sufficient. As an alternative, one may use much more computationally expensive dynamic ray tracing [2, 3].

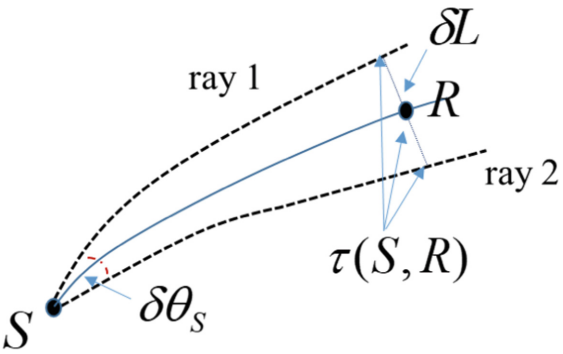


Fig. 4. Geometrical spreading calculation

4 Numerical Experiments

4.1 Lomax Ray Tracing Through a Salt Intrusion

Significant problems arise when the ray method calculates traveltimes below salt bodies. Salt bodies might have a very complex shape. Seismic wave velocities in salt are much higher than in sedimentary rocks surrounding a salt intrusion. Usually, it is very problematic to construct reliable rays passing through the salt body and calculate the corresponding traveltimes at those points of the medium that are located under the intrusion. As it is shown in [16, 21], frequency-dependent rays can help to solve this problem. Below we demonstrate that Lomax rays can penetrate through salt bodies successfully. Figure 5 shows a fragment of the well-known Sigsbee velocity model [25] with a salt body of complex shape (shown in yellow). Seismic wave velocity in salt is 4500 m/s meanwhile in surrounding area it doesn't exceed 3500 m/s. Point source is located near the surface, Zs = 20 m. Our task is to pass the rays through the salt intrusion and calculate the corresponding traveltimes in receivers located on the horizontal line in the depth below salt (Zr = 4100 m). For standard raytracing we used a code taken from well-known Seismic Unix freeware package [26]. Lomax rays are calculated using the code we developed. Figure 5a shows standard rays (black). As one can see, their behavior is irregular. At sharp, non-planar boundaries of the salt, the standard rays scatter. In the receiver line, where the first arrival traveltimes are calculated, "holes" are formed (i.e. intervals where the rays do not arrive at all). It is an obvious contradiction with the real physical process of wave propagation. Note that the rays are traced densely. Increment of the emerging angle from the source is very small (in this case, 0.02°). Maximum emerging angle is equal to 30° in this case. So totally 3000 rays were constructed (for illustrative purpose we plot each tenth ray in the figure). But it does not help to get the traveltimes on the entire line of receivers in depth. Figure 5b shows the Lomax rays calculated for a frequency of 5 Hz (shown in red). The parameter θ (smoothing aperture of local velocities) equals to 0.5 wavelength in each point of a ray. As one can see, Lomax rays' behavior is much more "physical" than the behavior of standard rays. Lomax rays pass through the salt body and arrive to receivers quite regularly. In Fig. 6 we compare first arrival traveltimes. Figure 6a demonstrates the traveltimes obtained

by the Lomax rays which are superimposed on the synthetic seismogram calculated by the finite-difference method for scalar wave-equation. For full wavefiled simulation we used a Ricker wavelet with a dominant frequency of 15 Hz. The Lomax rays traveltimes are marked with red circles. For comparison, we demonstrate the traveltimes provided by standard rays (blue circles). Lomax rays' traveltimes perfectly fits the first arrival in the seismogram. To demonstrate this fact more precisely, we show the first arrival traveltimes separately (Fig. 6b): the first arrival traveltimes picked from the synthetic seismogram are shown in blue; traveltimes according to Lomax rays are shown as red

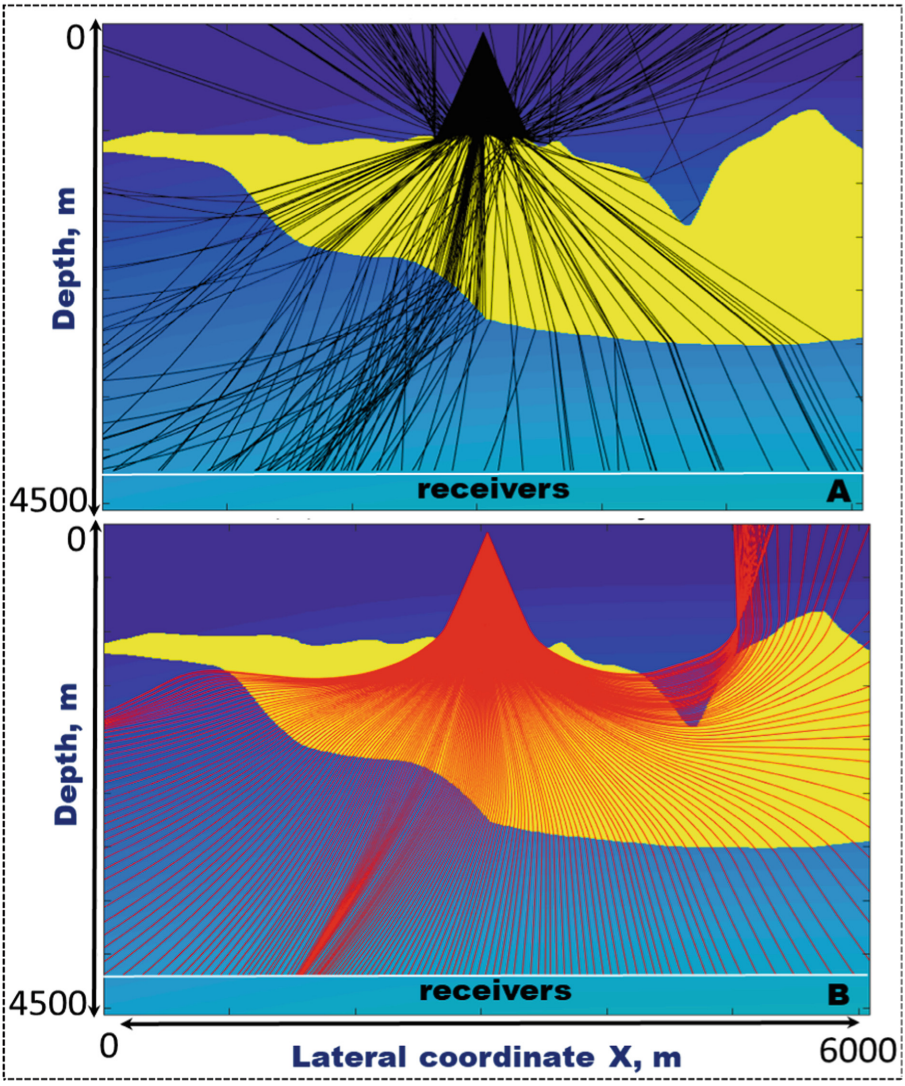


Fig. 5. Ray tracing in Sigsbee model. (a) Standard rays; (b) Lomax rays for frequency 5 Hz.

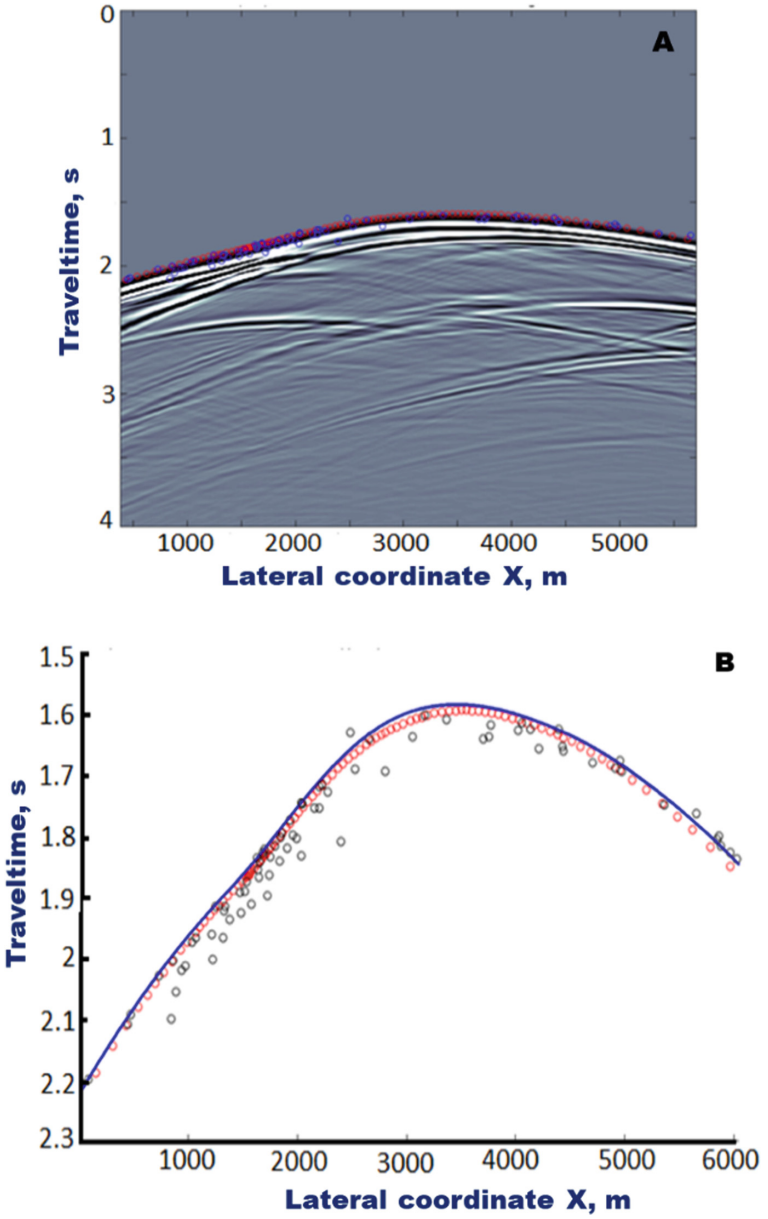


Fig. 6. (a) First arrival traveltimes along the Lomax rays (red circles) are superimposed on the synthetic common-shot gather; (b) comparison of first arrivals traveltimes: (blue) traveltimes computed by the finite difference method; (red circles) travel times along the Lomax rays calculated for frequency 5 Hz; (black) traveltimes along the standard rays. (Color figure online)

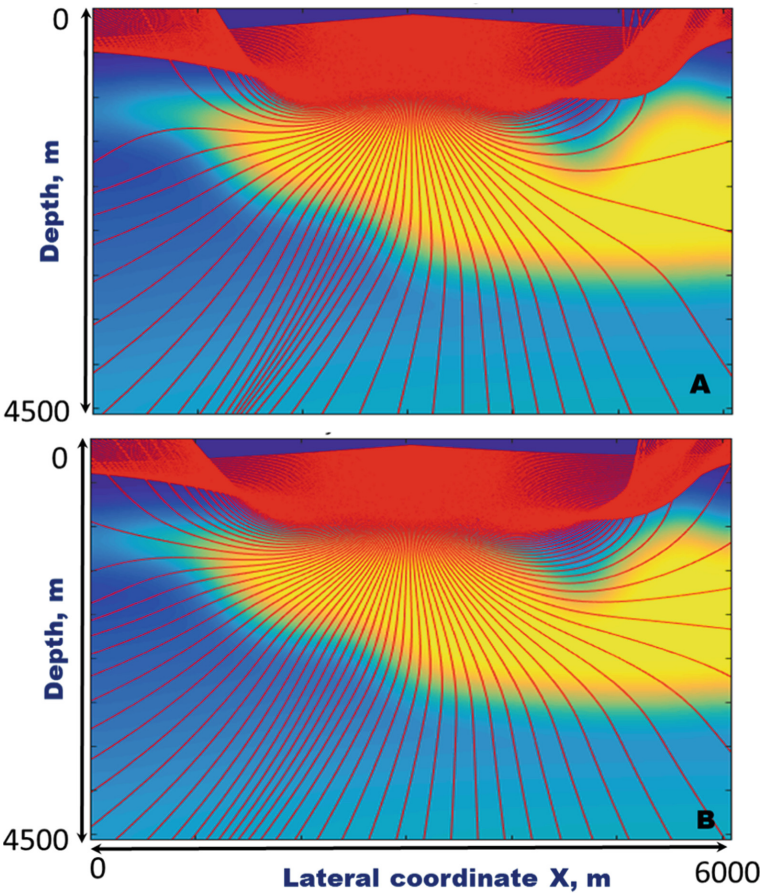


Fig. 7. Rays in the smoothed Segsbee model: (a) standard rays; (b) Lomax rays for a frequency of 10 Hz.

circles; traveltimes given by the standard rays are plotted as black circles. The residuals between the Lomax rays' traveltimes and exact traveltimes does not exceed 4 ms which can be considered quite satisfactory. Also important is the fact that the Lomax rays arrive at each receiver.

4.2 Ray-Based Wavefield Simulation in the Frequency Domain

Below, we present an example of acoustic wavefield simulation in the frequency domain using Lomax rays and compare results with the results provided by the standard finite difference method for acoustic wave equation. To simplify the comparison of results, in this example, we use a smoothed version of the Sigsbee velocity model (its fragment that was used in the previous example). Figure 7 shows a fragment of the smoothed Sigsbee model and the ray fields superimposed on it: Fig. 7a shows standard rays; Fig. 7b shows the Lomax ray constructed for a frequency 10 Hz. The parameter θ is equal to 0.5 wavelength in each point of a ray. Further, in Fig. 8 (left column) we show the traveltimes

calculated using the ray method in each point of the model after interpolation on a regular grid in comparison with the first arrival traveltimes got by the finite difference method. As one can see, the traveltimes calculated using standard rays have "holes" at the edges of the computational domain (i.e. there are no rays passed through these areas) (marked by the black ovals in Fig. 8b). Thus, although the velocity model is smooth, the standard ray method cannot provide reliable traveltimes. The traveltimes provided by the Lomax rays practically coincide with the first arrival "finite difference" traveltimes (residuals do not exceed 5 ms). In Fig. 8 (right column) we show the wavefields in the frequency domain for a fixed frequency 10 Hz (real part) which correspond to traveltime in the left column. As one can see, the wavefield constructed using the Lomax rays corresponds much better to the wave field calculated by the finite difference method than the result got using the standard rays. In Fig. 9, we compare the vertical and horizontal sections

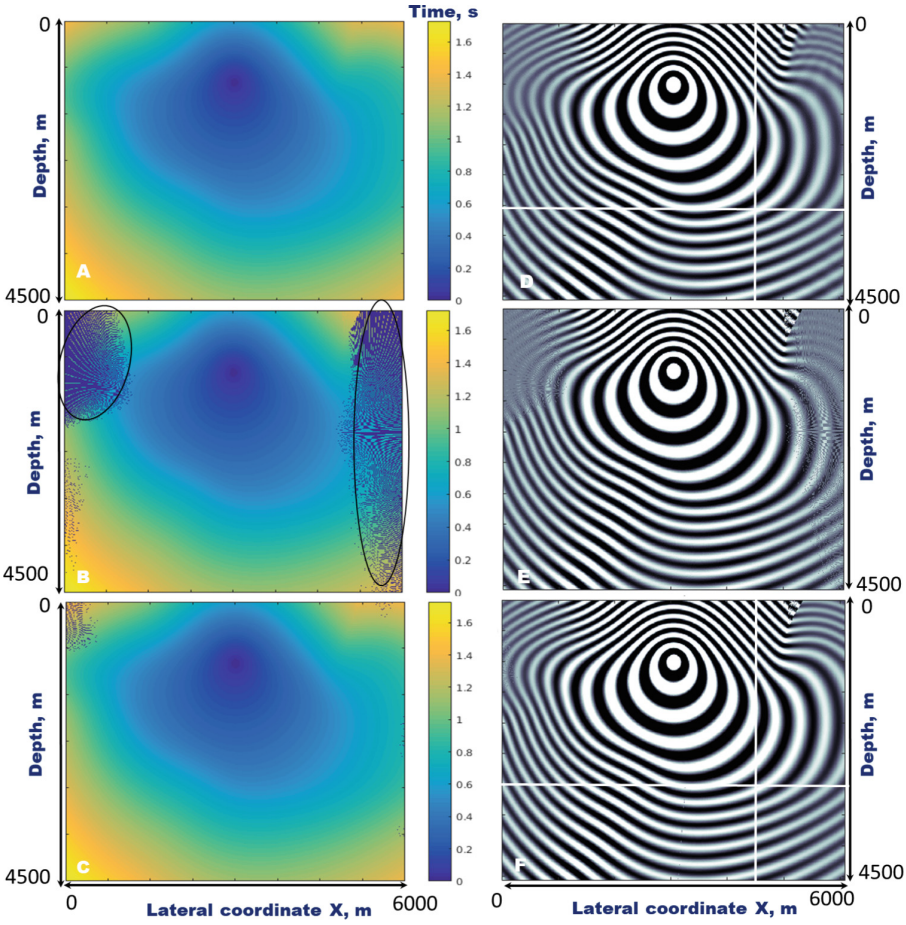


Fig. 8. (Left column) First arrival traveltimes distribution: (a) finite difference simulation; (b) standard ray method; (c) Lomax rays for a frequency of 10 Hz. (Right column) Corresponding wavefields for a fixed frequency 10 Hz: (d) FD simulation, (e) standard rays, (f) Lomax rays.

of the wavefields from Fig. 8d, 8f (corresponding locations are marked by the white lines) for the finite difference solution (shown in blue) and for the Lomax rays (red). Very satisfactory match is obvious. Thus, we show numerically that Lomax rays can effectively calculate wave-fields in fairly complex media.

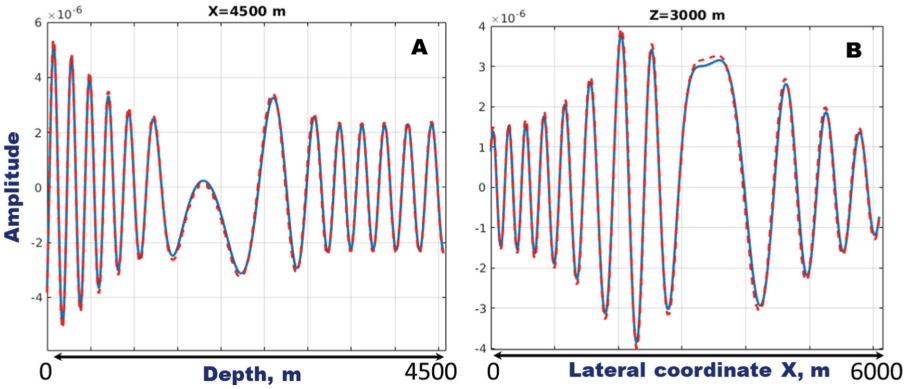


Fig. 9. Vertical (a) and horizontal (b) section of the wavefields from Fig. 8d, 8f: (blue) finite difference method, (red) Lomax rays. (Color figure online)

Table 1 summarizes the results of numerical experiments. We compare the computation time needed for wavefields simulation using the finite difference approach and ray methods. Also, we compare the relative error of the ray methods regarding finite difference modeling. One can see that the calculation time of the ray method, both using standard rays and Lomax rays, is several tens of times less than the calculation time of the finite difference method. The solution error provided by Lomax rays does not exceed 4% even for such a complex model as Sigsbee.

For a given rays' density, the construction of Lomax rays requires much more computational time than for standard rays. It is because at each time step along the Lomax ray multiple accesses to the velocity model (i.e. memory access) are required to calculate a value of the averaged velocity along the current position of the front. It will be especially problematic in 3D. Thus, in order to extend to 3D, the Lomax ray tracing code must be carefully optimized.

Table 1. Computational time for wavefield simulation for 1 source on 1 processor core in the Sigsbee model and the relative error of the ray method with respect to the result of finite difference modeling.

Method	Computational time	Relative error with respect to finite-difference modelling result
Finite-difference	~80 s	–
Standard rays	~2 s	7.5%
Lomax rays	~5 s	3.6%

5 Conclusion

In the paper, we consider "Lomax method" for calculating frequency-dependent rays. This method allows a simple and efficient approximation of a broadband signal propagation. We perform a comparative analysis of the Lomax method, the standard ray method and the finite difference method for calculating travel times and acoustic wavefields in complex media The relative error of wavefield calculated using Lomax rays regarding the finite difference solution is a percentage even for such a complex model as Sigsbee, while the computation time is more than an order of magnitude less in a two-dimensional case. Such results show the promise of using Lomax rays to calculate acoustic wavefields for solving inverse seismic problems in a three-dimensional environment.

Acknowledgments. The reported study was funded by RFBR and GACR, project number 20-55-26003.

References

1. Babich, V.M., Buldyrev, V.S.: Asymptotic Methods in Short-Wavelength Diffraction Theory. Alpha Science (2009)
2. Cerveny, V., Molotkov, I.A., Psencik, I.: Ray Theory in Seismology. Charles University Press, Prague (1977)
3. Cerveny, V.: Seismic Ray Theory. Cambridge University Press, Cambridge (2001)
4. Schneider, W.: Integral formulation for migration in two and three dimensions. Geophysics **43**, 49–76 (1978)
5. Bleistein, N.: On the imaging of reflectors in the earth. Geophysics **52**, 931–942 (1987)
6. Audebert, F., Nichols, D., Rekdal, T., Biondi, B., Lumley, D., Urdaneta, H.: Imaging complex geologic structure with single-arrival Kirchhoff prestack depth migration. Geophysics **62**, 1533–1543 (1997)
7. Kravtsov, Y., Orlov, Y.: Geometrical Optics of Inhomogeneous Media. Springer, Heidelberg (1990)
8. Ben-Menahem, A., Beydoun, W.B.: Range of validity of seismic ray and beam methods in general inhomogeneous media – I. General theory. Geophys. J. Int. **82**, 207–234 (1985)
9. Marquering, H., Dahlen, F.A., Nolet, G.: Three-dimensional sensitivity kernels for finite-frequency traveltimes: the banana-doughnut paradox. Geophys. J. Int. **137**, 805–815 (1999)
10. Dahlen, F.A., Hung, S.-H., Nolet, G.: Fréchet kernels for finite-frequency traveltimes—I. Theory. Geophys. J. Int. **141**, 157–174 (2000)
11. Cerveny, V., Soares, J.E.P.: Fresnel volume ray tracing. Geophysics **57**, 902–915 (1992)
12. Lomax, A.: The wavelength-smoothing method for approximating broad-band wave propagation through complicated velocity structures. Geophys. J. Int. **117**, 313–334 (1994)
13. Vasco, D.W., Peterson, J.E., Majer, E.L.: Beyond ray tomography: wavepaths and Fresnel volumes. Geophysics **60**, 1790–1804 (1995)
14. Bube, K.P., Washbourne, J.K.: Wave tracing: ray tracing for the propagation of band-limited signals: part 1 – theory. Geophysics **73**, VE377-VE384 (2008)
15. Protasov, M.I., Yarman, C.E., Nichols, D., Osypov, K., Cheng X.: Frequency-dependent ray-tracing through rugose interfaces. In: Proceedings of 2011 81st SEG Annual Meeting, pp. 2992–2996. SEG (2011)
16. Yarman, C.E., Cheng, X., Osypov, K., Nichols, D., Protasov, M.: Band-limited ray tracing. Geophys. Prosp. **61**, 1194–1205 (2013)

17. Vasco, D.W., Nihei, K.: Broad-band trajectory mechanics. Geophys. J. Int. **216**, 745–759 (2019)
18. Vasco, D.W., Nihei, K.T.: A trajectory mechanics approach for the study of wave propagation in an anisotropic elastic medium. Geophys. J. Int. **219**, 1885–1899 (2019)
19. Foreman, T.L.: An exact ray theoretical formulation of the Helmholtz equation. J. Acoust. Soc. Am. **86**, 234–246 (1989)
20. Protasov, M., Gadylshin, K.: Exact frequency dependent rays on the basis of Helmholtz solver, In: Proceedings of 2015 83rd SEG Annual Meeting, pp. 3739–3743. SEG (2015)
21. Protasov, M., Gadylshin, K.: Computational method for exact frequency-dependent rays on the basis of the solution of the Helmholtz equation. Geophys. J. Int. **210**, 525–533 (2017)
22. Chen, J., Zelt, C.A.: Comparison of full wavefield synthetics with frequency-dependent traveltimes calculated using wavelength-dependent velocity smoothing. J. Environ. Eng. Geophys. **22**, 133–141 (2017)
23. Virieux, J., Operto, S.: An overview of full-waveform inversion in exploration geophysics. Geophysics **78**, WCC1–WCC26 (2009)
24. Operto, M.S., Xu, S., Lambare, G.: Can we quantitatively image complex structures with rays. Geophysics **65**, 1223–1238 (2000)
25. Paffenholz J., Stefani, J., McLain, B., Bishop, K.: SIGSBEE_2A synthetic subsalt dataset - image quality as function of migration algorithm and velocity model error. In: Proceedings of 2002 64th EAGE Conference and Exhibition, cp-5–00108, EAGE (2002)
26. Cohen, J.K., Stockwell, Jr. J.W.: CWP/SU: Seismic Un*x Release No.39: an open source software package for seismic research and processing, Center for Wave Phenomena, Colorado School of Mines (2005)